Acta Materialia 116 (2016) 250–262

Contents lists available at ScienceDirect

Acta Materialia

journal homepage: www.elsevier.com/locate/actamat

Full length article

Effect of Si on the acceleration of bainite transformation by pre-existing martensite

Yuki Toji [a, *], Hiroshi Matsuda [a], Dierk Raabe [b]

[a] Steel Research Laboratory, JFE Steel Corporation, 1 Kawasaki-cho, Chuo-ku, Chiba 260-0835, Japan
[b] Max-Planck-Institut für Eisenforschung GmbH, Max-Planck-Str. 1, 40237 Düsseldorf, Germany

ARTICLE INFO

Article history:
Received 12 April 2016
Received in revised form
8 June 2016
Accepted 19 June 2016

Keywords:
Quenching & partitioning
Bainite
Martensite
Austenite
Atom probe tomography

ABSTRACT

Bainite transformation was investigated focusing on the influence of pre-existing martensite on the transformation kinetics, morphology and crystallographic orientation of subsequently formed bainite using EBSD and atom probe tomography. Two 1.1 wt% C-3wt.%Mn steels with and without 2 wt% Si were used to clarify the effect of Si. Steels were rapidly cooled from 900 °C to 300 °C and held at this temperature, or quenched from 900 °C once in water to generate approximately 30 vol% martensite followed by holding at 300 °C. Bainite transformation was clearly accelerated by pre-existing martensite in both Si-containing and Si-free steels. Bainite surrounds the pre-existing martensite in the Si-free steel, whereas it grows to the interior of the austenite grains in the steel containing 2 wt% Si. The major orientation relationship between bainite and adjacent austenite was changed by the presence of martensite from Nishiyama-Wassermann (N-W) to Greninger-Troiano (G-T) regardless of Si content. Clear carbon partitioning from martensite into austenite was observed prior to the bainite transformation in the 2 wt% Si steel, which was not observed in the Si-free steel. We suggest that the dislocations introduced by the martensite transformation act as a primary factor accelerating the bainite transformation when martensite is introduced prior to the bainite transformation.

1. Introduction

Quenching & partitioning (Q&P) steel is a promising candidate for automotive applications because an excellent balance of high tensile strength and good elongation can be obtained with chemical compositions similar to that of conventional transformation induced plasticity (TRIP) steels [1]. Transformation phenomena during the Q&P process are, however, not yet fully understood due to several reactions competing with carbon partitioning from martensite into austenite, which is the essential mechanism for stabilizing austenite in this process [1–5].

Bainite formation is one of the most frequently observed competing reactions in the Q&P heat treatment [6–10]. It seems to be difficult to preclude the bainite transformation during this heat treatment even with the addition of a large amount of alloying elements aiming at suppressing its formation [7]. This is presumably related to the phenomenon of bainite transformation being accelerated by martensite that forms before the bainite [11–20], since a certain amount of martensite is necessarily introduced before the partitioning step in the Q&P heat treatment. Therefore, the acceleration of bainite transformation by pre-existing martensite is an extremely important issue in the Q&P heat treatment.

Jellinghaus [11] reported that the bainite transformation at 300–400 °C was accelerated by pre-existing martensite formed at 150 °C in 0.86–1.21 wt% C steels. Goodenow et al. [12] also confirmed that pre-existing lower bainite accelerated upper bainite transformation in 0.31–0.69 wt% C steels. They suggested that the acceleration effect was mainly due to the transformation strain introduced by the lower bainite transformation since the annealing at temperatures above the bainite transformation start (Bs) temperature after the lower bainite reaction (for relaxing the strain) eliminates the acceleration effect. In addition to these studies, there are several reports which detected the acceleration of bainite transformation around the martensite transformation start (Ms) temperature [13–20].

Most previous studies on the above bainite acceleration effect dealt with steels of relatively low Si (~0.3 wt%) content, and there are few studies for steels with high Si content. Recently, Smanio

* Corresponding author.
E-mail address: y-toji@jfe-steel.co.jp (Y. Toji).

http://dx.doi.org/10.1016/j.actamat.2016.06.044
1359-6454/

et al. [21] studied the effect of partial martensite transformation on bainite reaction kinetics in high carbon steels with 0.24 wt% Si and 1.23 wt% Si using dilatometry. Gong et al. [22] reported the acceleration of bainite transformation by prior martensite in nano-bainite steel with 1.51 wt% Si content by means of dilatometry and neutron diffraction measurements. There is, however, no systematic study focusing on the effect of Si on the acceleration of bainite transformation by pre-existing martensite. Si is well known to suppress cementite formation. This effect is essential for Q&P steels [1–3] as well as for low-alloy TRIP steels [23–26] for acquiring the retained austenite by accumulating carbon in the austenite. High Si addition is expected to enhance the carbon partitioning from pre-existing martensite into surrounding austenite, which is speculated to affect the following bainite transformation.

Therefore, this study aims at clarifying the effect of Si on the acceleration of bainite transformation by pre-existing martensite via atomic-scale analysis using atom probe tomography.

2. Experimental procedure

2.1. Model alloy and processing

Two 1.1 wt% C-3wt% Mn steels with and without 2 wt% Si were used in this study to clarify the effect of Si. The chemical compositions of the steels are listed in Table 1. The Ms temperatures of these steels measured by dilatometry were almost the same as shown in the table. The steels were prepared by vacuum induction melting. The ingots were homogenized at 1240 °C for 172.8 ks, then air cooled to room temperature. The homogenized ingots were reheated and held at 1200 °C for 1.8 ks followed by hot rolling to sheets with a thickness of 3.6 mm, then air cooled to room temperature. Specimens with dimensions of 15 mm × 50 mm, cut from the hot rolled steel sheet, were then heat-treated according to Fig. 1. Fig. 1a shows a normal austempering treatment at 300 °C for bainite transformation, hereafter referred to as “austempering treatment”. Here specimens were rapidly cooled from 900 °C to 300 °C at a cooling rate of approximately 50 °C/s. The holding time at 900 °C was 180 s. In the heat treatment shown in Fig. 1b, specimens were quenched once in water (approximately 15 °C) to generate a certain amount of martensite followed by holding at 300 °C for bainite transformation, hereafter referred to as “Q&P treatment”. In this heat treatment, we can investigate bainite transformation in the case with pre-existing martensite. It should be noted that the thermal history during this heat treatment is the same as the quenching and tempering heat treatment since the quench temperature here is the water temperature. However, the transformation phenomena of the investigated steels in this heat treatment are not the same as the conventional quenching and tempering steel. Enough austenite remains in the investigated steels after water quenching (shown later) so that the carbon partitioning from martensite into austenite during holding at 300 °C is expected. Therefore, we describe this heat treatment as “Q&P treatment” in this study. Furthermore, selecting the water temperature as the quench temperature in the Q&P process is beneficial for the direct observation of microstructures before the partitioning step [4].

Table 1
Chemical compositions of steels used (wt.%).

Steel	C	Si	Mn	Al	Fe	[a]Ms (°C)
0Si	1.08	0.01	3.0	0.053	Bal.	32
2Si	1.07	2.2	2.9	0.048	Bal.	41

[a] Ms: Martensite transformation start temperature.

Although slight decarburization occurred near the surface during homogenization and reheating, it was confirmed that the carbon concentration at least at one quarter of the thickness of the heat-treated sheets was identical to the bulk carbon concentration. Therefore, all of the following characterization steps were performed at one quarter of the thickness of the heat-treated sheets to avoid the decarburized surface layer.

2.2. Microstructure characterization

Dilatation was probed using a Bähr Dil805 instrument to measure the Ms temperature and to investigate the volume change during holding at 300 °C. Samples for the dilatation measurement were taken from one quarter of the thickness of the hot-rolled or the water-quenched steels with dimensions of 4 mm × 9 mm × 1 mm. To measure the Ms temperature, the samples were heated and held at 900 °C for 180 s followed by rapid cooling to room temperature using hydrogen gas. The cooling rate from 900 °C to 100 °C was approximately 200 °C/s.

Microstructures in the cross section perpendicular to the transverse direction (TD cross section) etched with 0.1–0.3% nital were observed by optical microscopy and scanning electron microscopy (SEM). Electron backscatter diffraction (EBSD) measurements were performed with a step size of 40–50 nm to investigate the crystallographic orientation relationship between phases.

Atom probe tomography (APT) [27–38] was applied for the near-atomic quantitative investigation of carbon partitioning during holding at 300 °C after water quenching. Samples for APT measurements were prepared using focused ion beam (FIB) milling. APT analyses were performed using a local electrode atom probe (LEAP 3000X HR, Cameca Instruments) in voltage mode at a specimen temperature of around 65 K. The pulse fraction and the pulse rate were 15% and 200 kHz, respectively. Data analyses were performed using the IVAS software (Cameca Instruments). The acquired mass spectra revealed peaks corresponding to C^{+}, C^{2+}, C_2^{+}, C_3^{+}, C_3^{2+}, C_4^{2+}, Fe^{2+}, Si^{2+}, Mn^{2+}, Al^{2+} and Al^{3+}. In most of the analyses, the $(^{12}C_3^{13}C)^{2+}$ peak at a mass-to-charge ratio (Da) of 24.5 was detected. This means that the peak at 24 Da, 25 Da and 26 Da could be due to either C_2^{+} or C_4^{2+}, or a mixture of both [39–41]. Therefore, a peak decomposition algorithm supplied by the IVAS software was applied to decompose these peaks.

3. Results

3.1. Effect of pre-existing martensite and silicon addition on kinetics and morphology of bainite

Fig. 2 shows dilatations of the Si-free steel (Fig. 2a) and 2 wt% Si steel (Fig. 2b) during holding at 300 °C directly cooled from 900 °C (green curve: without martensite) or reheated after water quenching (red curve: with martensite), respectively. Fig. 2c and d represent the transformation ratio, which is defined as the dilatation at each time divided by the maximum dilatation during holding at 300 °C for each steel and heat treatment. The transformation was clearly accelerated when the specimens were subjected to water quenching (WQ) prior to holding at 300 °C in both steels. It should be noted that the scale of the abscissa axis used for the 2 wt% Si steel (Fig. 2b,d) is four times larger than that used for the Si-free steel (Fig. 2a,c). Hence, the transformation rate of 2 wt% Si steel is much more sluggish compared to that of Si-free steel [42].

Optical micrographs of the Si-free steel directly held at 300 °C (Fig. 3a–d) or reheated to 300 °C after water quenching (Fig. 3e–h) are shown in Fig. 3. In the case of the austempering treatment, only thinly-etched fresh martensite was observed at 720 s, which generated during the final quenching after holding at 300 °C. Slight

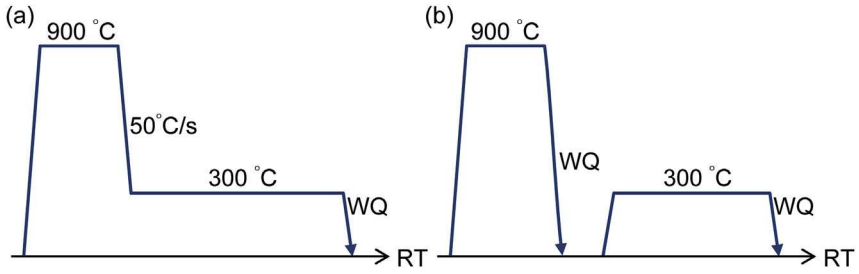

Fig. 1. Schematic diagram of heat treatments; (a) austempering heat treatment, (b) Q&P heat treatment. RT: room temperature, WQ: water quenching.

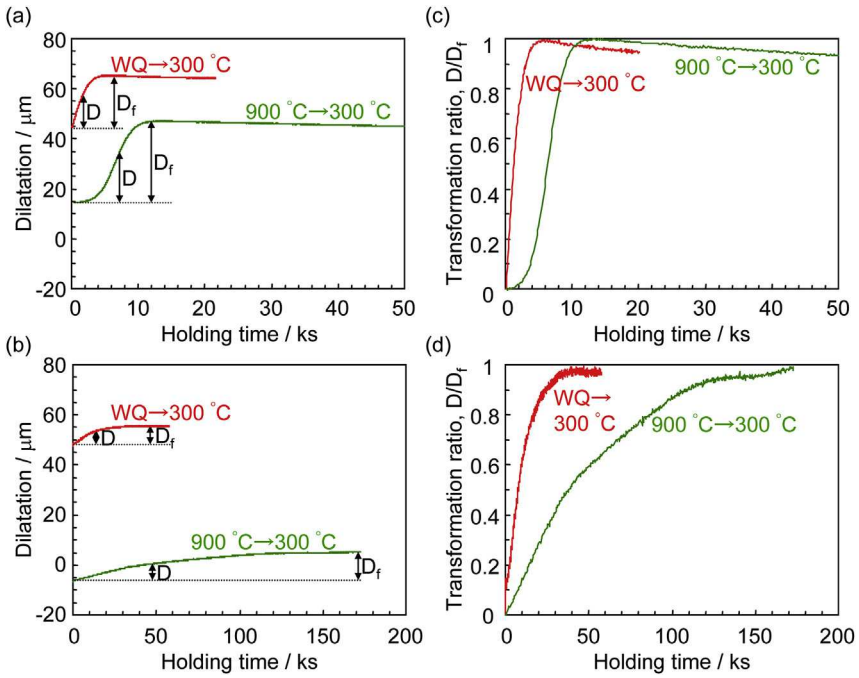

Fig. 2. Dilatation of 0Si steel (a) and 2Si steel (b) during holding at 300 °C directly quenched from 900 °C (green curve: without martensite) or reheated after WQ (red curve: with martensite). (c), (d) represents bainite transformation ratio, i.e., the dilatation at each time (D) divided by the maximum dilatation (D_f) during holding at 300 °C for each steel and heat treatment. WQ: water quenching. (For interpretation of the references to colour in this figure legend, the reader is referred to the web version of this article.)

nucleation of grains with black contrast, corresponding to bainite, was detected at 2.16 ks (Fig. 3b, the background microstructure here is, again, the fresh martensite). This transformation product increased for longer holding times, 3.6 ks (Fig. 3c) and 7.2 ks (Fig. 3d). Transformation proceeded much faster in the Q&P treatment (Fig. 3e–h). In this case, a certain amount of martensite exists before holding at 300 °C. The martensite generated during the first quenching (pre-existing martensite) was tempered during 10 s holding at 300 °C and is more darkly etched than that generated during the final quenching after holding at 300 °C (Fig. 3f). The volume fraction of the pre-existing martensite measured by the image analysis of Fig. 3f was approximately 30%. This martensite seems to become thicker for longer holding times (Fig. 3g,h), which is presumably caused by the bainite formation around the pre-existing martensite. Detailed microstructures are shown later. Fig. 4 shows optical micrographs of 2 wt% Si steel. In the case of the Q&P treatment, the relatively large plates with black contrast are the tempered pre-existing martensite and the tiny gray ones are the bainite (Fig. 4g,h). Similar to the case of Si-free steel, transformation was much faster with the presence of pre-existing martensite (Fig. 4e–h) compared to that without pre-existing martensite (Fig. 4a–d). However, the shape of bainite was different from that in Si-free steel, i.e., a nodular shape in Si-free steel and a plate shape in 2 wt% Si steel. Transformation rate of bainite was much lower in 2 wt% Si steel than that in Si-free steel especially in the case of the austempering treatment; there was still a very limited number of transformation products at 21.6 ks of holding in 2 wt% Si steel (Fig. 4b).

SEM micrographs of the initial state of transformation at 300 °C in Si-free steel are shown in Fig. 5. In the case of the austempering treatment, nodular transformation products consisting of ferrite and cementite were observed (Fig. 5a). This kind of transformation product has been reported mainly in hypereutectoid steels [43–47]. Most researchers regard it as a kind of bainite, referring to it as “columnar bainite” or “nodular bainite” [44–47]. In the case with the pre-existing martensite, the martensite was tempered at the beginning of the holding as is recognized by the carbide precipitation inside it (Fig. 5c). After holding for 720 s (Fig. 5d), another constituent can be observed surrounding the pre-existing martensite. There are plenty of carbides inside this new constituent. Hence, this is considered to be a similar type of bainite as that observed in the specimen without the pre-existing martensite. Fig. 6 shows SEM micrographs of 2 wt% Si steel. Plate-shaped bainite, which should be lower bainite [47], can be observed in

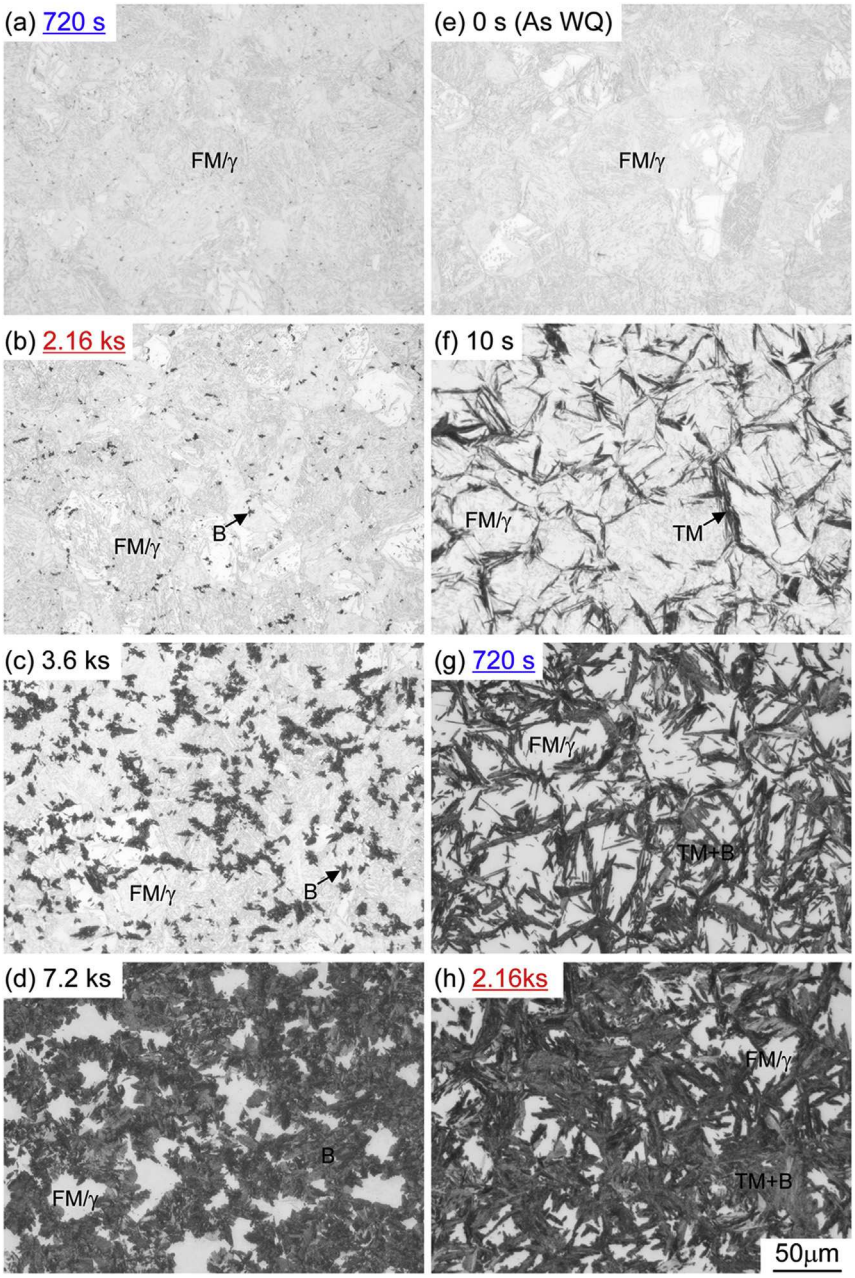

Fig. 3. Optical micrographs of 0Si steel directly held at 300 °C (a–d) or reheated to 300 °C after water quenching (e–h). Holding time at 300 °C is (a) 720 s, (b) 2.16 ks, (c) 3.6 ks, (d) 7.2 ks, (e) 0 s (As WQ), (f) 10 s, (g)720 s, (h)2.16 ks. FM: fresh martensite, γ: austenite, B: bainite, TM: tempered martensite. WQ: water quenching.

the specimen directly held at 300 °C for 21.6 ks (Fig. 6a). At a longer holding time, the fraction of bainite increased, but the shape did not change substantially (Fig. 6b). In the case with pre-existing martensite (Fig. 6c,d), small pieces of plate-shaped bainite can already be observed at 720 s (Fig. 6c). Unlike in the case of Si-free steel (Fig. 5d), the bainite here does not surround the pre-existing martensite; it tends to grow into the interior of the austenite grains.

3.2. *Effect of pre-existing martensite on crystallographic orientation relationship*

In order to analyze the influence of pre-existing martensite on the crystallographic orientation relationship between bainite and its parent austenite, the axis–angle representation of misorientations between bainite and austenite was applied. Table 2 shows the axis–angle values calculated for the exact Kurdjumov–Sachs (K-S), Nishiyama-Wassermann (N-W), Greninger-Troiano (G-T) and Bain orientation relationships (ORs) [48,49]. Fig. 7 shows SEM microstructures and corresponding OR maps superimposed on the image quality maps of specimens with and without pre-existing martensite in Si-free steel. The tolerance angle in this analysis was set as 2°. Note that the regions with low image quality indicated as FM in Fig. 7b,d are fresh martensite generated during the final quenching or sample preparation for SEM observation, and which are not clearly etched in the SEM images (Fig. 7a,c). In the case without martensite, the OR of most interfaces between the bainite and adjacent austenite is a N-W relationship as indicated by green lines (Fig. 7b). On the other hand, the major OR

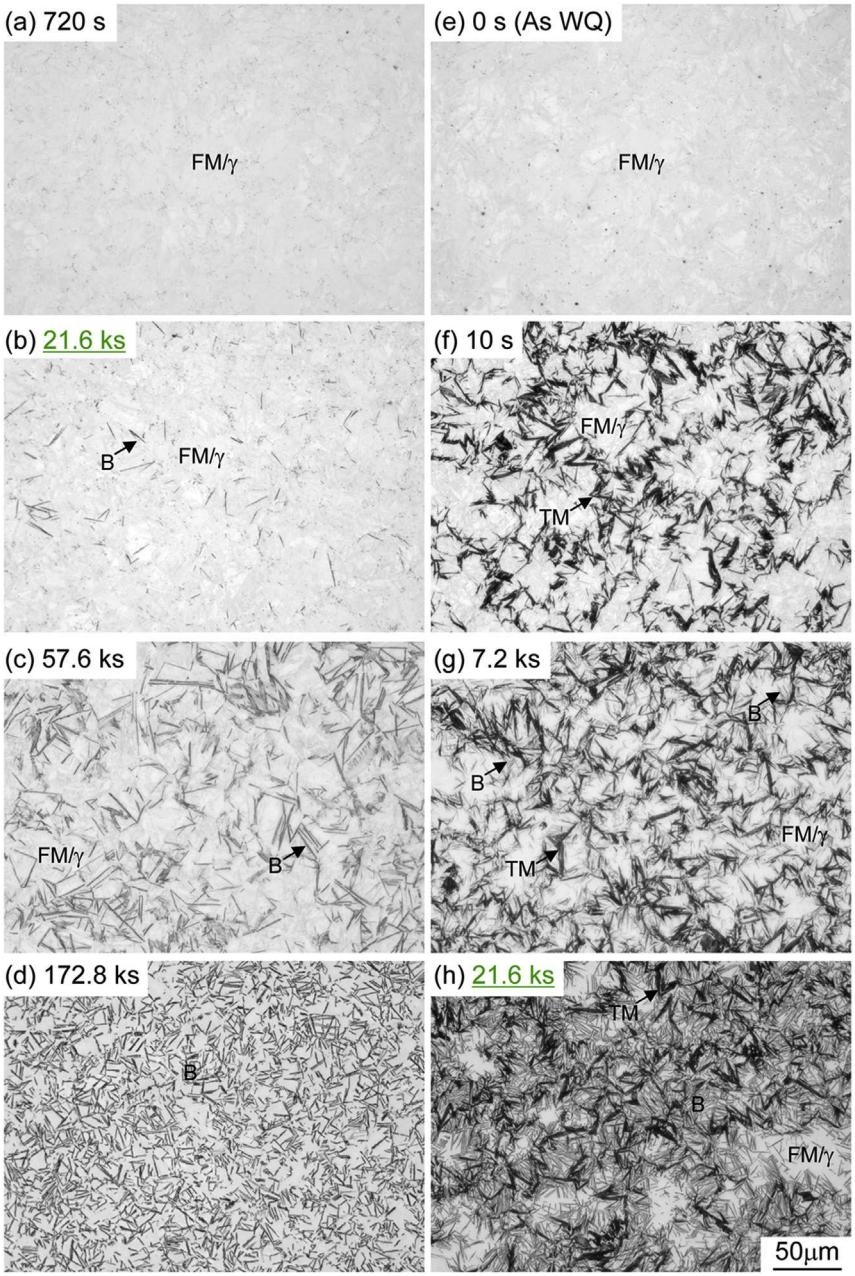

Fig. 4. Optical micrographs of 2Si steel directly held at 300 °C (a–d) or reheated to 300 °C after water quenching (e–h). Holding time at 300 °C is (a) 720 s, (b) 21.6 ks, (c) 57.6 ks, (d) 172.8 ks, (e) 0 s (As WQ), (f) 10 s, (g)7.2 ks, (h)21.6 ks. FM: fresh martensite, γ: austenite, B: bainite, TM: tempered martensite. WQ: water quenching.

turns to G-T (expressed as blue lines) in the case with pre-existing martensite (Fig. 7d). The fresh martensite mentioned above also has a G-T relationship with the austenite. Fig. 7e shows the inverse pole figure (IPF) map of the bcc phases. The orientation of bainite is nearly the same as that of the adjacent martensite. A similar effect of pre-existing martensite can be recognized in 2 wt% Si steel (Fig. 8) even though the morphology of the bainite is very different. In Fig. 8c, the dark-etched thin plates are bainite (B), etched thick plates with relatively high image quality (Fig. 8d) are (pre-existing) tempered martensite (TM), and thick plates with low image quality, which are not clearly etched in the SEM image, are fresh martensite (FM), respectively. Here, we can recognize the OR between the pre-existing tempered martensite and adjacent austenite as G-T, since the pre-existing martensite is not covered with bainite in the case of 2 wt% Si steel, unlike the case of Si-free steel. What is different from the case of Si-free steel is that the orientation of bainite does not seem to be the same as that of the adjacent martensite, though it is difficult to indicate the adjacent martensite for each of bainite since they seem to be slightly away from the martensite (Fig. 8e). Fig. 9 summarizes the influence of pre-existing martensite on the ORs between the bainite and adjacent austenite. The length fraction here means the value that the length of the interface between the bainite and austenite (B/A interface), which has each OR, is divided by the total length of the B/A interface. It should be noted that the sum of the fractions of these three ORs is more than 100%. Some interfaces can be counted as having two or three ORs since the difference among these ORs is not that large. As shown in Figs. 7 and 8, N-W is the major OR without pre-existing martensite in

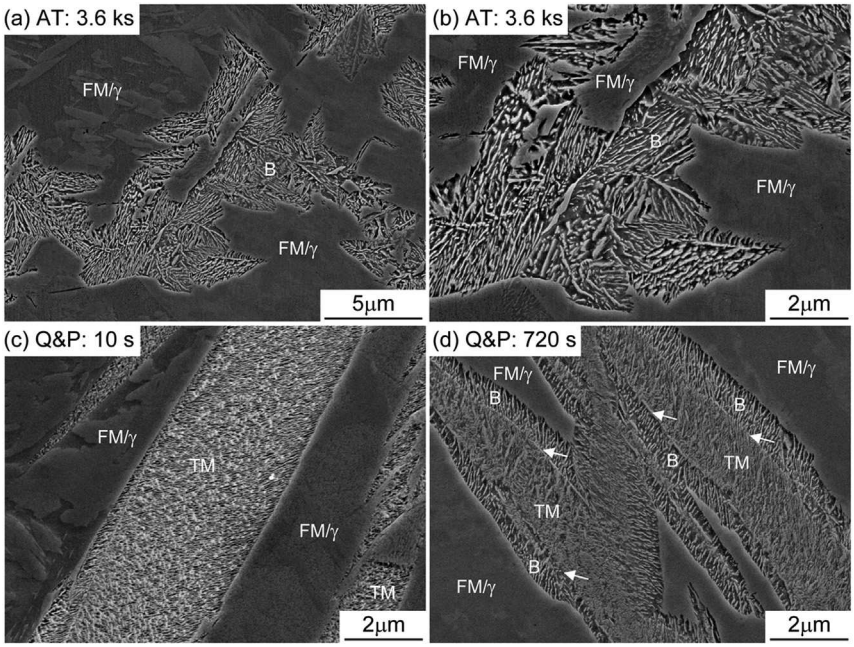

Fig. 5. SEM micrographs of 0Si steel directly held at 300 °C (a,b) or reheated to 300 °C after water quenching (c,d). Holding time at 300 °C is (a)(b) 3.6 ks, (c) 10 s, (d) 720 s (b) is the higher magnification image of (a). AT: austempering treatment, Q&P: quenching & partitioning treatment, FM: fresh martensite, γ: austenite, B: bainite, TM: tempered martensite. Arrows indicate the interfaces between pre-existing (tempered) martensite and bainite.

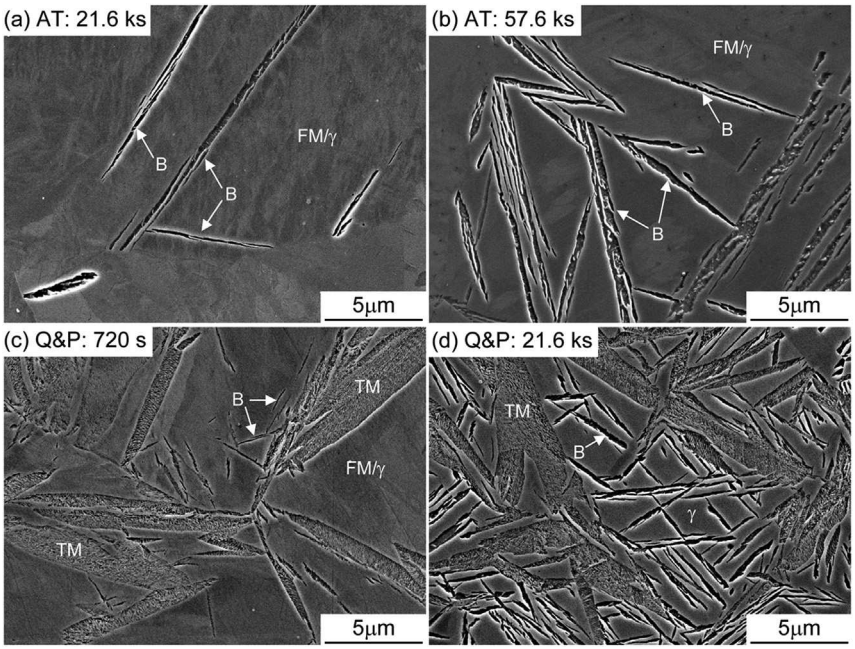

Fig. 6. SEM micrographs of 2Si steel directly held at 300 °C (a,b) or reheated to 300 °C after water quenching (c,d). Holding time at 300 °C is (a) 21.6 ks, (b) 57.6 ks, (c) 720 s, (d) 21.6 ks. AT: austempering treatment, Q&P: quenching & partitioning treatment, FM: fresh martensite, γ: austenite, B: bainite, TM: tempered martensite.

Table 2
Axis–angle values for different orientation relationships (ORs) between bainite (B) and austenite (γ).

ORs between B and γ	Axis	Angle
K-S	42.85	⟨17.8 17.8 96.8⟩
G-T	44.26	⟨12.2 18.4 97.5⟩
N-W	45.99	⟨8.3 20.1 97.6⟩
Bain	45.00	⟨0 0 1⟩

both steels. If martensite is introduced prior to bainite, the major OR changes to G-T.

3.3. Effect of carbon partitioning from pre-existing martensite

Carbon partitioning from pre-existing martensite can have some influence on the subsequent bainite transformation. Therefore, the carbon partitioning behavior was investigated by means of APT. Figs. 10a and 11a show the carbon atom maps of the initial state

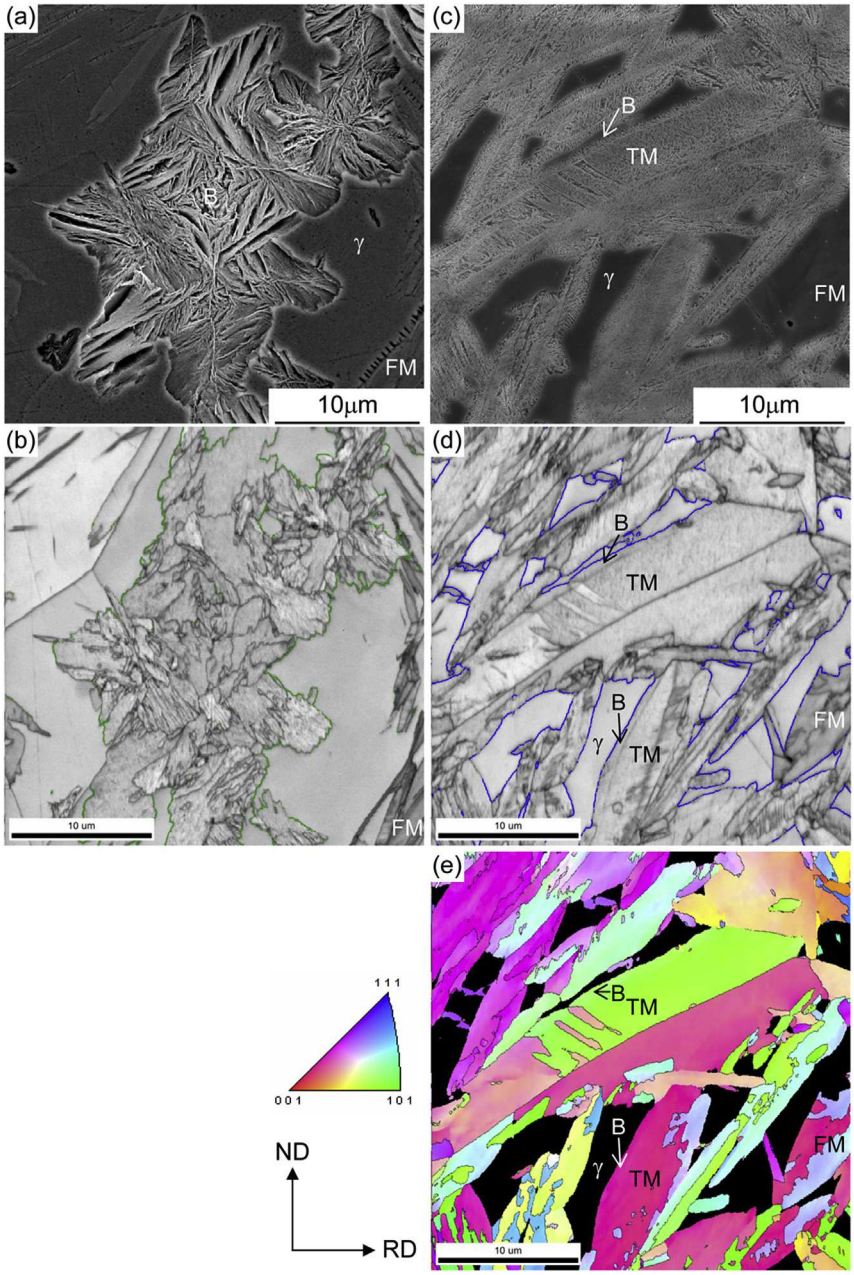

Fig. 7. SEM microstructures (a,c), corresponding OR maps (b,d) and bcc IPF map (e) of 0Si steel directly held at 300 °C for 7.2 ks (a,b) and reheated to 300 °C for 720 s after water quenching (c–e). Green and blue lines indicate N-W and G-T OR, respectively. Tolerance angle in this analysis was set as 2°. γ: austenite, B: bainite, FM: fresh martensite, TM: tempered martensite (pre-existing martensite). (For interpretation of the references to colour in this figure legend, the reader is referred to the web version of this article.)

(10 s) of holding at 300 °C after water quenching in Si-free and 2 wt % Si steels, respectively. At this stage, bainite did still not clearly form even in Si-free steel (Fig. 5c) in which bainite transformation is faster than that in 2 wt% Si steel. The top regions of these maps are austenite and the bottom regions are martensite. Carbides already formed in martensite at 10 s of holding in both steels. Figs. 10b and 11d show the carbon and manganese concentration profiles along the arrow indicated in Figs. 10a and 11a, respectively. At first, manganese did not partition at all between the phases in both steels. In Fig. 10b, the ferrite carbon concentration in the martensite region is nearly zero due to the carbide precipitation in this region, whereas the austenite carbon concentration is around the bulk carbon concentration although the values vary because of the small analyzed volume. In contrast, carbon partitioning into austenite from martensite is clearly observed in the vicinity of the interface between the abutting phases in the 2 wt% Si steel (Fig. 11d). What is interesting here is that the austenite carbon concentration near the interface does not appear to be uniform. The carbon concentration in austenite very close to the carbide (indicated as (2) in Fig. 11a,c, 6.2 at.%) is slightly less than that away from the carbide (indicated as (1) in Fig. 11a,b, 6.7 at.%).

4. Discussion

Bainite transformation is clearly accelerated by the presence of pre-existing martensite in the 2 wt% Si steel as well as in the Si-free steel, consistent with the observations presented in Refs. [21,22]. This phenomenon can be utilized to shorten the required heat

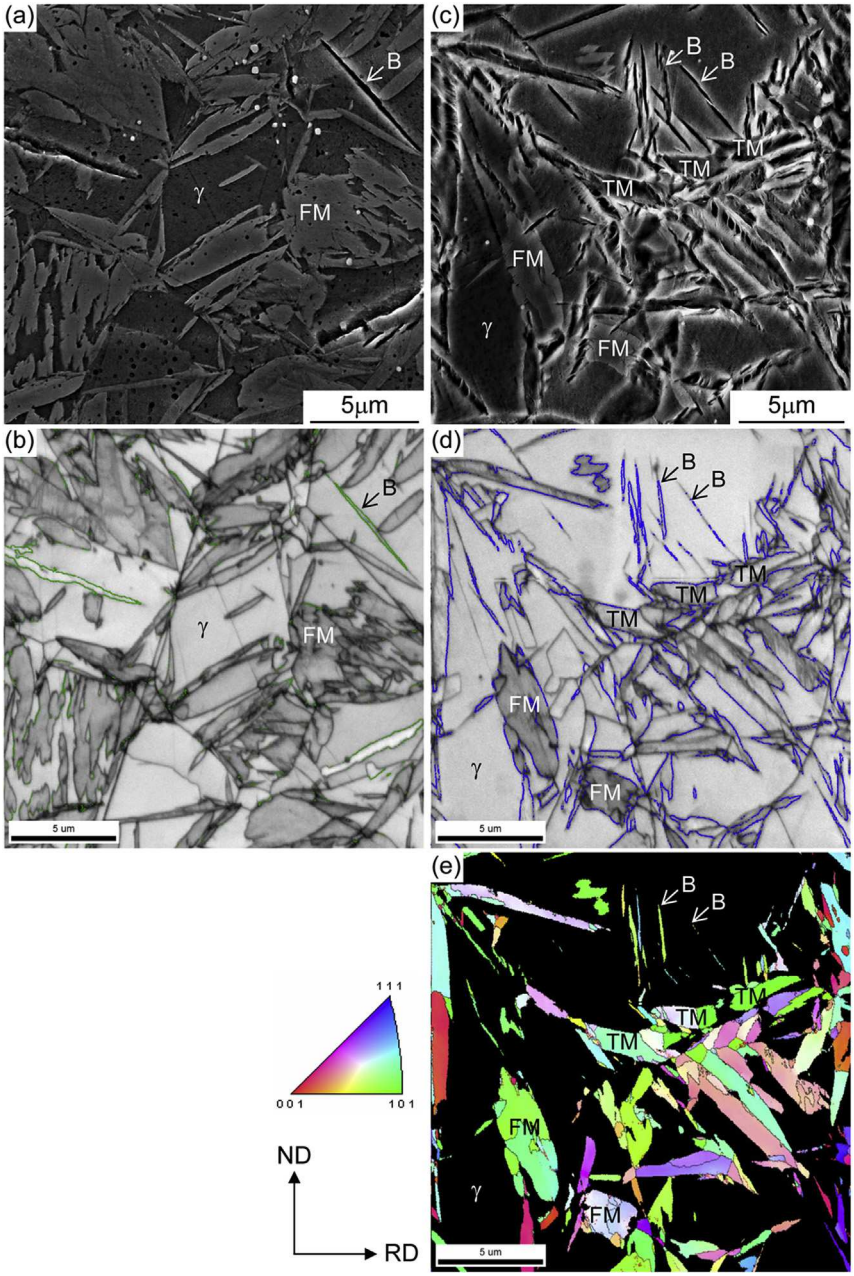

Fig. 8. SEM microstructures (a,c), corresponding OR maps (b,d) and bcc IPF map (e) of 2Si steel directly held at 300 °C for 21.6 ks (a,b) and reheated to 300 °C for 2.16 ks after water quenching (c–e). Green and blue lines indicate N-W and G-T OR, respectively. Tolerance angle in this analysis was set as 2°. γ: austenite, B: bainite, FM: fresh martensite, TM: tempered martensite (pre-existing martensite). (For interpretation of the references to colour in this figure legend, the reader is referred to the web version of this article.)

treatment time for stabilizing austenite in Si-containing TRIP steels, for instance, in continuous annealing lines, in which the heat treatment time is generally not so long. This effect is more profound in the case of super bainite [50,51], because the required time for bainite transformation at low temperatures (~300 °C) is usually very long, as is the case of alloys with high carbon content and low Ms temperature investigated in this study. A small amount of pre-existing martensite can render the transformation time one order of magnitude shorter than that without pre-existing martensite.

It is obvious that the pre-existing martensite can shorten (or eliminate) the incubation time for the following bainite transformation as shown in this study (Fig. 2) and previous reports [20–22]. On the other hand, the effect of the pre-existing martensite on bainite transformation kinetics is not yet clear. Smanio et al. [21] concluded that the kinetics of bainite transformation after prior formation of a given fraction of martensite is identical to those observed after formation of the same fraction of bainite from the comparison of dilatation curves of the investigated steels. Fig. 12 compares the dilatation curves in this study, which are arranged in the same way as Smanio et al. [21]. The volume fraction of the pre-existing martensite is approximately 30% as mentioned before. In the case of the Si-free steel (Fig. 12a), the dilatation curve with pre-existing martensite is shifted toward that without pre-existing martensite by the dilatation corresponding to 30 vol% bainite determined from the dilatation curve. In the case of the 2 wt% Si steel without pre-existing martensite (Fig. 12b), bainite transformation is not yet finished even after 172.8 ks holding. Therefore, the holding time when the volume fraction of bainite is

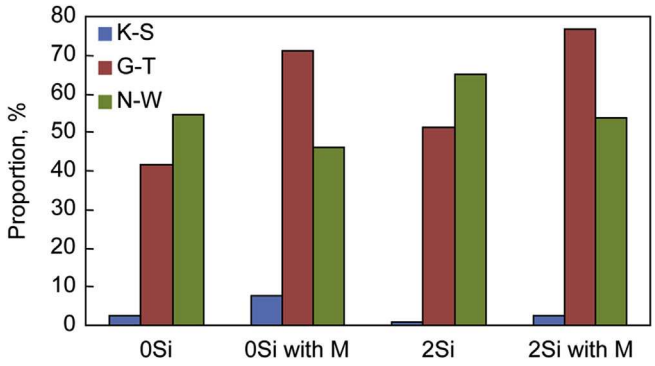

Fig. 9. Influence of pre-existing martensite on the crystallographic orientation relationship between bainite and prior austenite. M: martensite.

30% is determined by the metallography, namely, the volume fraction of bainite is approximately 30% at 57.6 ks holding by the image analysis of Fig. 4c. The bainite transformation kinetics of the Si-free steel with 30 vol% pre-existing martensite is similar to that after formation of the same fraction of bainite (Fig. 12a), consistent with the previous report [21]. However, the bainite transformation rate of the 2 wt% Si steel with pre-existing martensite is clearly larger than that after 30 vol% bainite formation without pre-existing martensite. This can be also confirmed by the microstructure observation (Fig. 4). The amount of newly formed bainite during 21.6 ks holding from 10 s (Fig. 4f, with approx. 30 vol% martensite) to 21.6 ks (Fig. 4h) is obviously more than that during 115.2 ks holding from 57.6 ks (Fig. 4c, with approx. 30 vol% bainite) to 172.8 ks (Fig. 4d). The above difference between steels with and without Si is attributed to the difference in the carbon partitioning

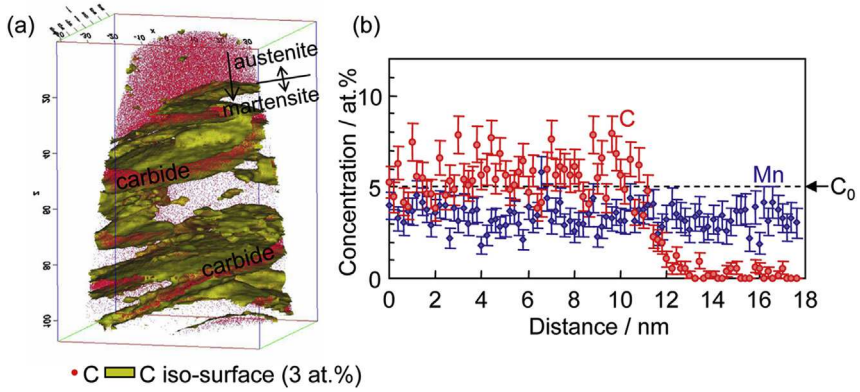

Fig. 10. Carbon atom map of 0Si steel held at 300 °C for 10s after water quenching (a). Carbon (C), manganese (Mn) concentration profiles along the arrow indicated in the carbon atom map (a) are shown in (b). The yellow surfaces in (a) are the iso-concentration surfaces with 3 at.% C. The error bars in (b) represent the one-sigma statistical error. C_0: bulk carbon content. (For interpretation of the references to colour in this figure legend, the reader is referred to the web version of this article.)

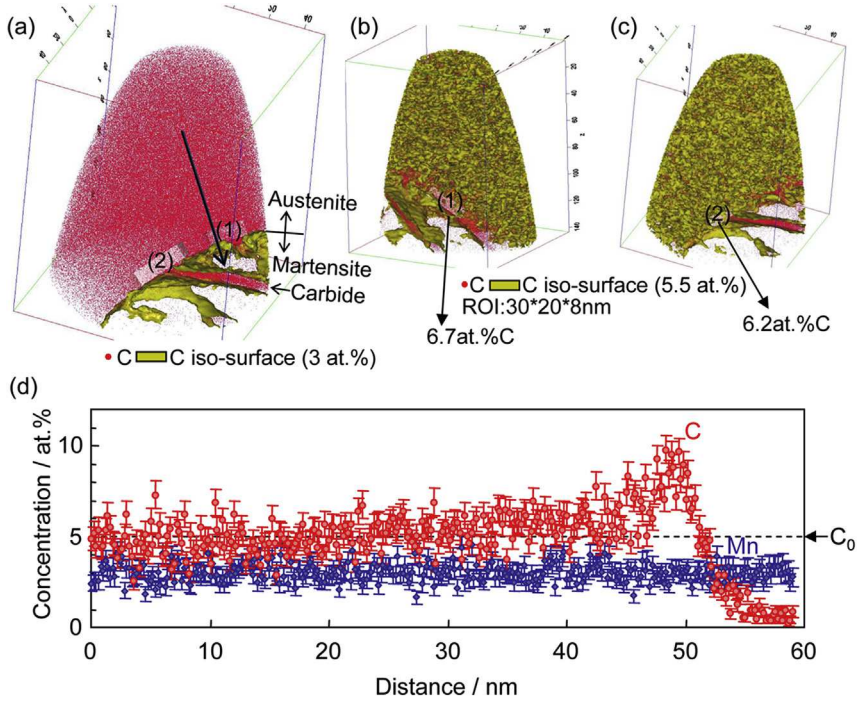

Fig. 11. Carbon atom maps of 2Si steel held at 300 °C for 10s after water quenching (a–c). Carbon (C), manganese (Mn) concentration profiles along the arrow indicated in the carbon atom map (a) are shown in (d). The yellow surfaces in (a~c) are the iso-concentration surfaces with 3 at.% C for (a) and 5.5 at.% C for (b) and (c), respectively. The error bars in (d) represent the one-sigma statistical error. C_0: bulk carbon content.

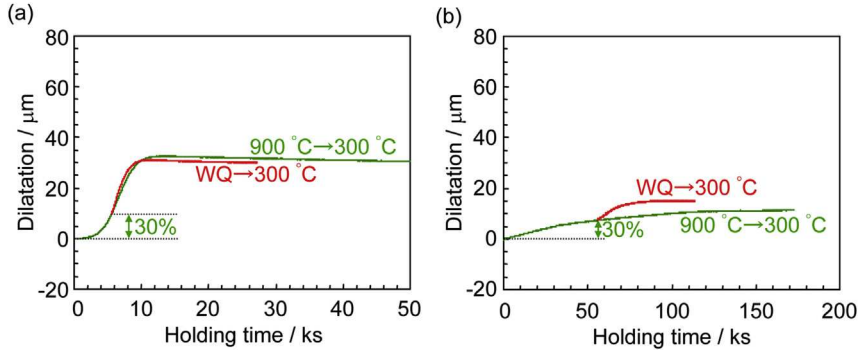

Fig. 12. Comparison of the dilatation curves with and without pre-existing martensite (approximately 30 vol%) in (a) 0Si steel and (b) 2Si steel. The dilatation curves with pre-existing martensite are shifted toward those without pre-existing martensite by the dilatation corresponding to 30 vol% bainite. WQ: water quenching.

behavior from bainite or pre-existing martensite into austenite during holding at 300 °C. In the Si-free steel, carbides precipitated in bainite and pre-existing martensite (Fig. 5), and carbon partitioning from these phases to the surrounding austenite can be ignored (Fig. 10). Therefore, the same volume fraction of bainite and pre-existing martensite does not affect the carbon concentration in the surrounding austenite and hence the subsequent bainite formation. In the 2 wt% Si steel, carbides did not precipitate in the bainite (Fig. 6), which means that most carbon partitioned from bainite to the surrounding austenite. In contrast, a certain amount of carbides precipitated in the pre-existing martensite in the 2 wt% Si steel as shown in Fig. 6, though the carbon partitioning from pre-existing martensite was also observed (Fig. 11). Hence, the carbon enrichment into the surrounding austenite from the pre-existing martensite is considered to be lower than that from the same fraction of bainite. The chemical driving force for bainite transformation becomes lower with an increase in the carbon concentration in austenite. Therefore, the bainite transformation kinetics was higher with the pre-existing martensite than that with the same fraction of bainite in the 2 wt% Si steel. The difference between this study and the report of Smanio et al. [21] can be due to the difference in alloy composition and/or heat treatment conditions. Garcia-Mateo et al. [52] reported that the carbon concentration in bainitic ferrite increased with lowering the transformation temperature, resulting in the less carbon partitioning from bainitic ferrite to surrounding austenite. This phenomenon can reduce the difference between the carbon partitioning from martensite and that from bainite, which may equalize the effect of the same amount of martensite and bainite on the bainite transformation kinetics, though it is not clear.

Regarding the mechanisms of the acceleration of bainite transformation by pre-existing martensite, two mechanisms have been proposed. One is that the transformation strain introduced by martensite formation provides preferential nucleation sites for subsequent bainite transformation, and the other is that the interface between the pre-existing martensite and austenite acts as a preferential nucleation site. Most researchers have supported the first idea although there is no clear evidence for this mechanism yet available. Howard et al. [14] investigated the isothermal transformation around the Ms temperature using 0.75–1.35C-0.3Si-0.5Mn-0~5.3Ni (wt.%) steels, and observed the acceleration of bainite just below the Ms temperature (75–200 °C depending on the chemical composition). The microstructure consisted of lenticular martensite and plate-shaped bainite. They mentioned that the effect of the martensite-austenite interface may be only a secondary factor since much of the premature bainite forms “in the clear” away from the martensite plate, and that the austenite deformation caused by the martensite formation stimulates the subsequent bainite transformation. Goodenow et al. [12] also confirmed that pre-existing lower bainite accelerated upper bainite transformation in 0.31–0.69 wt% C steels. They suggested that the acceleration effect was mainly due to the transformation strain introduced by the lower bainite transformation since the annealing above the bainite start (Bs) temperature after the lower bainite reaction (for relaxing the strain) eliminates the acceleration effect. On the other hand, Kawata et al. [20] recently claimed that the interfacial energy is a more important factor for the acceleration effect. They investigated the crystallographic orientation of pre-existing martensite and bainite in 0.2–0.4 wt% C-2.5 wt% Mn with and without 8 wt% Ni steels. In their study, bainite formation was observed along the pre-existing martensite in the 8 wt% Ni steel and the misorientation between bainite and adjacent martensite was only 2.4°. They also compared the bainite transformation acceleration effect by pre-existing martensite (with transformation strain) and pre-existing ferrite (without transformation strain), and concluded that the influence of strain was small since the acceleration effect of martensite and ferrite was the same level when the volume fraction of each phase was the same. For this line of interpretation, the area fraction of the interface between pre-existing phases and austenite should, however, be supposedly more important than the volume fraction of the pre-existing phases, which does not seem to be the same in their report since the shape and size of the pre-existing ferrite and martensite is significantly different. As mentioned above, the mechanism of the bainite acceleration effect caused by the pre-existing phases is still under debate.

Fig. 13 summarizes the influence of the pre-existing martensite and Si addition on the nucleation site and morphology of bainite obtained in this study. Comparing the present study with previous reports, the Si-free steel exhibited microstructural and orientation features that are similar to those reported by Kawata et al. [20], though the type of pre-existing martensite seems to be different, i.e., lath martensite in their report and lenticular martensite in this study. On the other hand, the 2 wt% Si steel showed a similar microstructure to that reported by Howard et al. [14]. Some bainite seem to form not on the interface between martensite and austenite but away from the pre-existing martensite. It should be, however, noted that even though the bainite is away from the martensite in the observed surface, we have to consider the microstructure in three dimensions, since the bainite can touch a pre-existing martensite beneath the observed surface [53].

Another point to be discussed here is that the bainite morphology was nodular in the Si-free steel whereas it was plate in the 2 wt% Si steel, regardless of the presence of the pre-existing martensite. Spanos et al. [47] reported the transition from nodular to lower bainite (plate-like or acicular morphology) in

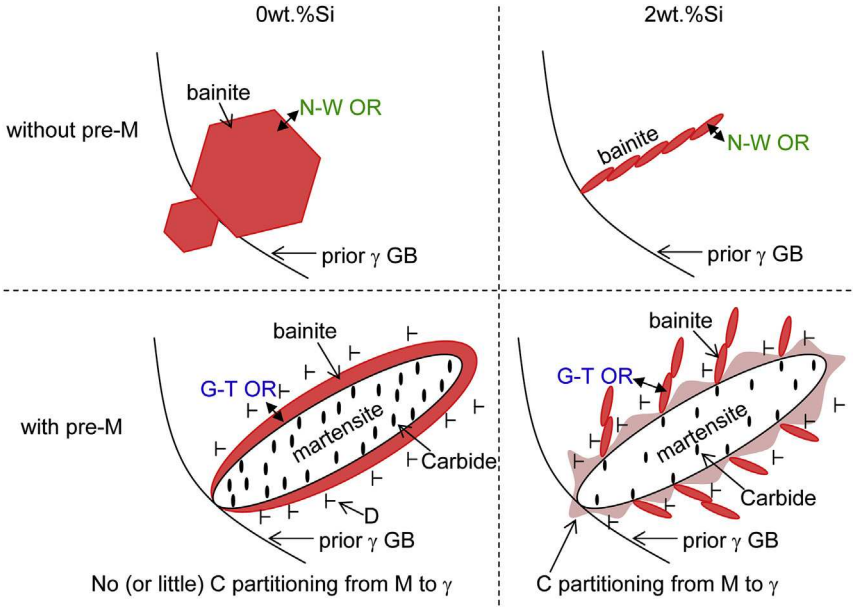

Fig. 13. Schematic diagram expressing the influence of pre-existing martensite and Si on the morphology of bainite. pre-M: pre-existing martensite, γ: austenite, OR: orientation relationship, GB: grain boundary, C: carbon. D: dislocation introduced by martensite transformation.

steels that did not contain Si. They proposed that the transition was caused by the difference in the driving force for nucleation of ferrite and cementite. If the driving force of ferrite nucleation is much greater than that of cementite, the bainite morphology becomes plate-like, for example, by lowering the transformation temperature. In this context, the influence of Si on the morphology at the same transformation temperature (300 °C in the present case) can be similarly speculated, i.e., Si reduces the driving force for cementite nucleation relative to that for ferrite nucleation, which is considered to be the reason why the morphology of bainite changes with the Si content.

Regarding the OR between the bainite and adjacent austenite, the major OR was changed by the presence of martensite from N-W to G-T (Fig. 13). The OR between the pre-existing martensite and austenite was G-T as mentioned before (Fig. 8d). Therefore, the orientation of bainite seems to be regulated by the adjacent martensite. Similar orientation regulation effects by pre-existing martensite have been reported in Refs. [20,22]. The trend was the same regardless of the Si content. Therefore, it is speculated that the same mechanism operated in both steels with and without Si even though the morphology of the bainite is profoundly different.

According to the APT analysis of the initial state (10 s) of holding at 300 °C after water quenching in the Si-free and 2 wt% Si steels, carbon partitioning from pre-existing martensite into austenite prior to bainite transformation was not observed in the Si-free steel, whereas it was clearly observed in the 2 wt% Si steel. This difference is probably due to the fact that the carbide precipitation in martensite was retarded in the 2 wt% Si steel compared to the Si-free steel so that a portion of the carbon atoms could partition into austenite in the 2 wt% Si steel. Here, it should be noted that the carbon concentration in the austenite near the interface in the 2 wt % Si steel was, at least locally, already higher than the carbon concentration corresponding to T_0 point (hereafter referred to as "T_0 concentration") for the 2 wt% Si steel at 300 °C (5.44 at.%). In the case of the displacive mechanism, the bainite transformation is considered to stop when the austenite carbon concentration reaches the T_0 concentration because there is no driving force for transformation from fcc to bcc without carbon diffusion if the austenite carbon concentration is above the T_0 concentration [54]. Therefore, it is unlikely for bainite to nucleate very close to the martensite in the case of the 2 wt% Si steel. This is presumably also the reason why the bainite seemed to exist slightly away from the pre-existing martensite and did not surround the pre-existing martensite in the 2 wt% Si steel unlike the case of the Si-free steel (Figs. 5 and 6). Furthermore, the austenite carbon concentration near the interface was not uniform (Fig. 11). This is attributed to the fact that the carbon atoms near the carbide were consumed when forming the carbide so that the amount of carbon atoms that could be enriched in the austenite was decreased near the carbide. Therefore, we suggest that bainite nucleates in the regions where there are less carbon atoms in the austenite, for example, in the vicinity of carbides, as illustrated in Fig. 13.

These results and considerations suggest that bainite nucleation is accelerated both, by the strain introduced during the martensite transformation and also by the interfacial energy between pre-existing martensite and austenite. If Si is not added and carbon partitioning from martensite to austenite does not occur prior to the bainite transformation, the bainite nucleates either directly on the interface, or it grows to touch the interface soon after its nucleation by dissociation of existing dislocations, as proposed by Olson and Cohen [55] for martensite transformation. This is due to the fact that the nucleation directly on the interface or sharing the interface soon after nucleation can reduce more energy than in the case where bainite does not touch the interface between martensite and austenite. If enough Si is added to retard carbide precipitation and consequently carbon partitions from martensite to austenite prior to bainite transformation, bainite nucleates in the regions slightly away from the pre-existing martensite through the dissociation of dislocations introduced by martensite transformation. Some of the nucleated bainite will touch the interface between martensite and austenite, and others will grow to the interior of the austenite grains. As mentioned earlier, the orientation regulation mechanism by pre-existing martensite was the same regardless of Si addition. This implies that the mechanism of the acceleration of bainite transformation by pre-existing martensite are the same in both steels. Therefore, we suggest that

the dislocations introduced by martensite transformation are profoundly contributing to the bainite acceleration phenomenon caused by the pre-existing martensite even in the Si-free steel as well as in the 2 wt% Si steel. The results in this study are, however, not enough to conclude which is the major factor for the acceleration effect, the strain caused by the pre-existing martensite or the interface between martensite and austenite, and thus further studies are required.

5. Summary

Bainite transformation, which is one of the competing reactions that take place during the partitioning step in the Q&P process, was investigated focusing on the effect of pre-existing martensite on bainite transformation kinetics and crystallographic orientation, especially in steel with high Si content (2 wt%) compared with Si-free steel. Bainite transformation was clearly accelerated by the pre-existing martensite in both Si-containing and Si-free steels. Bainite surrounds the pre-existing martensite in the Si-free steel, whereas it grows to the interior of the austenite grains in the 2 wt% Si steel. The major orientation relationship between bainite and adjacent austenite was changed by the presence of martensite from N-W to G-T regardless of Si addition. Clear carbon partitioning from martensite to austenite was observed prior to bainite transformation in 2 wt% Si steel, which was not observed in Si-free steel. The results obtained in this study suggest that the dislocations introduced by martensite transformation are profoundly contributing to the bainite acceleration phenomenon caused by the pre-existing martensite.

Acknowledgement

We would like to express our deep gratitude to Prof. K. Tsuzaki, Kyushu University, Dr. G. Miyamoto, Tohoku University, Dr. N. Nakada, Tokyo Institute of Technology, and Dr. M. Koyama, Kyusyu University, for insightful comments and suggestions. Dr. P-P. Choi and Dr. M. Herbig, Max-Planck-Institut für Eisenforschung GmbH, are gratefully acknowledged for helpful discussion on the atom probe tomography data.

References

[1] J.G. Speer, A.M. Streicher, D.K. Matlock, F.C. Rizzo, G. Krauss, Quenching and partitioning: a fundamentally new process to create high strength TRIP sheet microstructure, in: E.B. Damm, M. Merwin (Eds.), Austenite Formation and Decomposition, TMS/ISS, Warrendale, 2003, pp. 505–522.
[2] J.G. Speer, D.K. Matlock, B.C. De Cooman, J.G. Schroth, Carbon partitioning into austenite after martensite transformation, Acta Mater. 51 (2003) 2611–2622.
[3] J.G. Speer, D.V. Edmonds, F.C. Rizzo, D.K. Matlock, Partitioning of carbon from supersaturated plates of ferrite, with application to steel processing and fundamentals of the bainite transformation, Curr. Opin. Solid State Mater. Sci. 8 (2004) 219–237.
[4] Y. Toji, H. Matsuda, M. Herbig, P.P. Choi, D. Raabe, Atomic-scale analysis of carbon partitioning between martensite and austenite by atom probe tomography and correlative transmission electron microscopy, Acta Mater. 65 (2014) 215–228.
[5] Y. Toji, G. Miyamoto, D. Raabe, Carbon partitioning during quenching and partitioning heat treatment accompanied by carbide precipitation, Acta Mater. 86 (2015) 137–147.
[6] M.J. Santofimia, T. Nguyen-Minh, L. Zhao, R. Petrov, I. Sabirov, J. Sietsma, New low carbon Q&P steels containing film-like intercritical ferrite, Mater. Sci. Eng. A 527 (2010) 6429–6439.
[7] M.J. Santofimia, L. Zhao, R. Petrov, C. Kwakernaak, W.G. Sloof, J. Sietsma, Microstructural development during the quenching and partitioning process in a newly designed low-carbon steel, Acta Mater. 59 (2011) 6059–6068.
[8] K. Seto, H. Matsuda, Application of nanoengineering to research and development and production of high strength steel sheets, Mater. Sci. Technol. 29 (2013) 1158–1165.
[9] M.J. Santofimia, L. Zhao, J. Sietsma, Microstructural evolution of a low-carbon steel during application of quenching and partitioning heat treatments after partial austenitization, Metall. Mater. Trans. A 40 (2009) 46–57.
[10] E.J. Seo, L. Cho, B.C. De Cooman, Application of quenching and partitioning (Q&P) processing to press hardening steel, Metall. Mater. Trans. A 45 (2014) 4022–4037.
[11] W. Jellinghaus, Anregung der Zwischenstufen-Umwandlung des Stahles durch kleine Mengen von α-Eisen, Arch. Eisenhütt 23 (1952) 459–470.
[12] R.H. Goodenow, R.H. Barkalow, R.F. Hehemann, Bainite transformations in hypoeutectoid steels, in: Physical Properties of Martensite and Bainite, Special Report 93, Iron and Steel Institute, London, 1969, pp. 135–141.
[13] H. Lange, K. Mathieu, Ueber den Ablauf der Austenitumwandlung im unterkühlten Zustand bei Eisen-Nickel-Kohlenstoff-Legierungen, Mitt, KWI Eisenforsch. 20 (1938) 125–134.
[14] R.T. Howard, M. Cohen, Austenite transformation above and within the martensite range, Trans. AIME 176 (1948) 384–397.
[15] S.V. Radcliffe, E.C. Rollason, The kinetics of the formation of bainite in high-purity iron-carbon alloys, J. Iron Steel Inst. 191 (1959) 56–65.
[16] B.N.P. Babu, M.S. Bhat, E.R. Parker, V.F. Zacky, A rapid magnetometric technique to plot isothermal transformation diagrams, Metall. Trans. A 7 (1976) 17–22.
[17] C.E. Ericsson, M.S. Bhat, E.R. Parker, V.F. Zackay, Isothermal studies of bainitic and martensitic transformations in some low alloy steels, Metall. Trans. A 7 (1976) 1800–1803.
[18] M. Oka, H. Okamoto, Swing back in kinetics near Ms in hypereutectoid steels, Metall. Trans. A 19 (1988) 447–452.
[19] H. Vetters, J. Dong, H. Bomas, F. Hoffmann, H.W. Zoch, Microstructure and fatigue strength of the roller-bearing steel 100Cr6 (SAE 52100) after two-step bainitisation and combined bainitic-martensitic heat treatment, Int. J. Mater. Res. 97 (2006) 1432–1440.
[20] H. Kawata, K. Hayashi, N. Sugiura, N. Yoshinaga, M. Takahashi, Effect of martensite in initial structure on bainite transformation, Mater. Sci. Forum 638–642 (2010) 3307–3312.
[21] V. Smanio, T. Sourmail, Effect of partial martensite transformation on bainite reaction kinetics in different 1%C steels, Solid State Phenom. 172–174 (2011) 821.
[22] W. Gong, Y. Tomota, S. Harjo, Y.H. Sua, K. Aizawa, Effect of prior martensite on bainite transformation in nanobainite steel, Acta Mater. 85 (2015) 243–249.
[23] S.J. Matas, R.F. Hehemann, The structure of bainite in hypoeutectoid steels, Trans. Met. Soc. AIME 221 (1961) 179–185.
[24] H.K.D.H. Bhadeshia, D.V. Edmonds, The bainite transformation in a silicon steel, Metall. Trans. A 10 (1979) 895–907.
[25] O. Matsumura, Y. Sakuma, H. Takechi, Enhancement of elongation by retained austenite in intercritical annealed 0.4C-1.5Si-0.8Mn steel, Trans. ISIJ 27 (1987) 570–579.
[26] Y. Sakuma, O. Matsumura, O. Akisue, Influence of C content and annealing temperature on microstructure and mechanical properties of 400 °C transformed steel containing retained austenite, ISIJ Int. 31 (1991) 1348–1353.
[27] A. Cerezo, T.J. Godfrey, G.D.W. Smith, Application of a position-sensitive detector to atom probe microanalysis, Rev. Sci. Instrum. 59 (1988) 862–866.
[28] M.K. Miller, A. Cerezo, M.G. Hetherington, G.D.W. Smith, Atom Probe Field Ion Microscopy, Oxford University Press, Oxford, 1996.
[29] K. Hono, Atom probe microanalysis and nanoscale microstructure in metallic materials, Acta Mater. 47 (1999) 3127–3145.
[30] M.K. Miller, Atom Probe Tomography Analysis at the Atomic Scale, Kluwer Academic/Plenum, New York, 2000.
[31] T.F. Kelly, M.K. Miller, Atom probe tomography, Rev. Sci. Instrum. 78 (2007) 031101.
[32] P.P. Choi, M. da Silva, U. Klement, T. Al-Kassab, R. Kirchheim, Thermal stability of electrodeposited nanocrystalline Co-1.1at.%P, Acta Mater. 53 (2005) 4473–4481.
[33] M.J. Duarte, J. Klemm, S.O. Klemm, K.J.J. Mayrhofer, M. Stratmann, S. Borodin, A.H. Romero, M. Madinehei, D. Crespo, J. Serrano, S.S.A. Gerstl, P.P. Choi, D. Raabe, F.U. Renner, Element-resolved corrosion analysis of stainless-type glass-forming steels, Science 341 (2013) 372–376.
[34] M. Herbig, D. Raabe, Y. Li, P.P. Choi, S. Zaefferer, S. Goto, Atomic-scale quantification of grain boundary segregation in nanocrystalline material, Phys. Rev. Lett. 112 (2014) 126103.
[35] M. Herbig, M. Kuzmina, C. Haase, R.K.W. Marceau, I. Gutierrez-Urrutia, D. Haley, D.A. Molodov, P.P. Choi, D. Raabe, Grain boundary segregation in Fe–Mn–C twinning-induced plasticity steels studied by correlative electron backscatter diffraction and atom probe tomography, Acta Mater. 83 (2015) 37–47.
[36] M. Kuzmina, D. Ponge, D. Raabe, Grain boundary segregation engineering and austenite reversion turn embrittlement into toughness: example of a 9 wt.% medium Mn steel, Acta Mater. 86 (2015) 182–192.
[37] M. Kuzmina, M. Herbig, D. Ponge, S. Sandlöbes, D. Raabe, Linear complexions: confined chemical and structural states at dislocations, Science 349 (2015) 1080–1083.
[38] L. Morsdorf, C.C. Tasan, D. Ponge, D. Raabe, 3D structural and atomic-scale analysis of lath martensite: effect of the transformation sequence, Acta Mater. 95 (2015) 366–377.
[39] Y. Li, P.P. Choi, C. Borchers, S. Westerkamp, S. Goto, D. Raabe, Atomic-scale mechanisms of deformation-induced cementite decomposition in pearlite, Acta Mater. 59 (2011) 3965–3977.
[40] Y. Li, P.P. Choi, S. Goto, C. Borchers, D. Raabe, R. Kirchheim, Evolution of strength and microstructure during annealing of heavily cold-drawn 6.3 GPa hypereutectoid pearlitic steel wire, Acta Mater. 60 (2012) 4005–4016.
[41] Y. Li, D. Raabe, M. Herbig, P.P. Choi, S. Goto, A. Kostka, H. Yarita, C. Borchers,

R. Kirchheim, Segregation stabilizes nanocrystalline bulk steel with near theoretical strength, Phys. Rev. Lett. 113 (2014) 106104.
[42] T. Sourmail, V. Smanio, Low temperature kinetics of bainite formation in high carbon steels, Acta Mater. 61 (2013) 2639–2648.
[43] A.B. Greninger, A.R. Troiano, Crystallography of austenite decomposition, Trans. AIME 140 (1940) 307–331.
[44] J.R. Vilella, Trans. AIME 140 (1940) 332–334.
[45] G.R. Speich, M. Cohen, Growth rate of bainite, Trans. AIME 218 (1960) 1050–1059.
[46] T.G. Nilan, Morphology and kinetics of austenite decomposition at high pressure, TMS-AIME 239 (1967) 898–909.
[47] G. Spanos, H.S. Fang, D.S. Sarma, H.I. Aaronson, Influence of carbon concentration and reaction temperature upon bainite morphology in Fe-C-2 Pct Mn alloys, Metall. Trans. A 21 (1990) 1391–1411.
[48] S. Zaefferer, J. Ohlert, W. Bleck, A study of microstructure, transformation mechanisms and correlation between microstructure and mechanical properties of a low alloyed TRIP steel, Acta Mater. 52 (2004) 2765–2778.
[49] H. Sato, S. Zaefferer, A study on the formation mechanisms of butterfly-type martensite in Fe–30% Ni alloy using EBSD-based orientation microscopy, Acta Mater. 57 (2009) 1931–1937.
[50] F.G. Caballero, H.K.D.H. Bhadeshia, J.A. Mawella, D.G. Jones, P. Brown, Design of novel high strength bainitic steels: Part 2, Mater. Sci. Technol. 17 (2001) 517–522.
[51] F.G. Caballero, H.K.D.H. Bhadeshia, Very strong bainite, Curr. Opin. Solid State Mater. Sci. 8 (2004) 251–257.
[52] C. Garcia-Mateo, J.A. Jimenez, H.W. Yen, M.K. Miller, L. Morales-Rivas, M. Kuntz, S.P. Ringer, J.R. Yangb, F.G. Caballero, Low temperature bainitic ferrite: evidence of carbon super-saturation and tetragonality, Acta Mater. 91 (2015) 162–173.
[53] C.C. Tasan, M. Diehl, D. Yan, C. Zambaldi, P. Shanthraj, F. Roters, D. Raabe, Integrated experimental–simulation analysis of stress and strain partitioning in multiphase alloys, Acta Mater. 81 (2014) 386–400.
[54] H.K.D.H. Bhadeshia, A rationalization of shear transformation in steels, Acta Metall. 29 (1981) 1117–1130.
[55] G.B. Olson, M. Cohen, A general mechanism of martensitic nucleation = Part I. General concepts and the FCC → HCP Transformation, Metall. Trans. A 7 (1976) 1897–1904.